Design of a Linear Bulk Superconductor Magnet Synchronous Motor for Electromagnetic Aircraft Launch Systems

Gorazd Štumberger, *Member, IEEE*, Mehmet Timur Aydemir, *Member, IEEE*, Damir Žarko, and Thomas A. Lipo, *Fellow, IEEE*

***Abstract*—High-temperature superconducting (HTS) material in bulk form is used to design a linear synchronous motor for an electromagnetic aircraft launch system. The motor is designed without an iron core. Stator coils are placed in the air while the permanent magnets used in conventional design of linear permanent magnet synchronous motors are replaced by the HTS bulk magnets. The physical, operational, and equivalent circuit parameters of the linear motor with HTS bulk magnets are compared with those of a linear permanent magnet synchronous motor and linear induction motor designed for the same application. Results show that utilizing superconducting magnets is only superior at temperatures below 40 K.**

***Index Terms*—Bulk superconductor, electromagnetic aircraft launch, linear motors.**

I. Introduction

FOLLOWING the invention of high-temperature superconducting (HTS) materials [1], application of superconductivity in various fields attracted many researchers. Present status and future projection of superconducting technologies including cables, magnetic energy storage, motors, generators, flywheel bearings, fault current limiters, transformers, and all superconducting substations are presented in [2]. HTS materials are used in bulk forms in magnetic bearing and levitation systems [3]. Field-cooled bulk YBCO materials can trap very high magnetic fields. A sample 25 mm in diameter and 13 mm in thickness can trap 3.7 T at 77 K, when field cooled in 5 T [4]. Trapped field value increases as the temperature is decreased. A flux density of 7.09 T at 29.8 K by using two 26-mm diameter YBCO bulk magnets has been reported [5]. Superconductive properties of the bulk materials can be improved by using different structures and doping technologies. For example, 14 T at 20 K has been reached by reinforcement of the superconductors using a steel tube and by adding Ag [6]. Also, increased values of trapped fields have been observed when Sm is used instead of Ba, along with some Ag [7]. Ag is added to the material to improve the mechanical strength of the bulk magnets [8]. Several levitation systems using bulk superconductor (BSC) magnets along with normal permanent magnets have been reported in the literature [9], [10]. These magnets have also been used in different motor applications, and promising results have been obtained [11]–[13]. The possibility of using HTS materials for electromagnetic launch systems was first considered in [14] for space applications. It was concluded that BSC magnets could be employed near 20 K, but operation above 30 K would require more understanding of the physics of the material. Later, the same idea was considered for electromagnetic aircraft launch systems [15]–[18] to replace the steam catapults currently in use. In this paper, the results of a design for a linear motor that uses BSC magnets instead of conventional permanent magnets are presented. The motor has been designed for use in an electromagnetic aircraft launch system. The results have been compared with those of a permanent magnet motor and a linear induction motor designed for the same application. It has been concluded that BSC magnets are only superior at temperatures below 40 K, and more development is needed in terms of material properties for use at high temperatures.

Manuscript received November 7, 2003. This paper was recommended by Associate Editor S. Schwenterly. This work was supported by the Office of Naval Research and performed at the University of Wisconsin, Madison.

G. Štumberger is with the Faculty of Electrical Engineering and Computer Science, University of Maribor, 2000 Maribor, Slovenia (e-mail: gorazd.stumberger@uni-mb.si).

M. T. Aydemir is with the Department of Electrical and Electronics Engineering, Gazi University, 06570 Ankara, Turkey (e-mail: aydemirmt@gazi.edu.tr).

D. Žarko and T. A. Lipo are with the Department of Electrical and Computer Engineering, University of Wisconsin, Madison, WI 53706-1691 USA (e-mail: zarko@cae.wisc.edu; lipo@engr.wisc.edu).

Digital Object Identifier 10.1109/TASC.2004.824342

II. Design Problem

The problem considered in this work is to design a motor to be used in an electromagnetic aircraft launch system (EMALS) [15]–[18]. The system is composed of a linear motor, power electronic components, and a control system designed to accelerate an aircraft to its take off speed and then to abruptly stop the moving rotor portion. The time lapse between two takeoffs is 45 s. Design parameters used are as follows: $\mathrm{aircraft\ mass} = 23\,000$ kg, fly away speed $v = 103$ m/s, maximal available path for acceleration $= 94.49$ m (310 ft) and the maximal available path for deceleration $= 5.79$ m (19 ft).

Neglecting all kinds of friction, motion of the entire system can be described by

$$m\frac{d^2z}{dt^2} = F \quad \text{or} \quad ma = F \tag{1}$$

where m is the mass of the moving part of the entire system, z is the rotor position, and F is the force required for acceleration a. The mass to be accelerated is the sum of the aircraft mass and the rotor mass. The mass to be decelerated is only the rotor

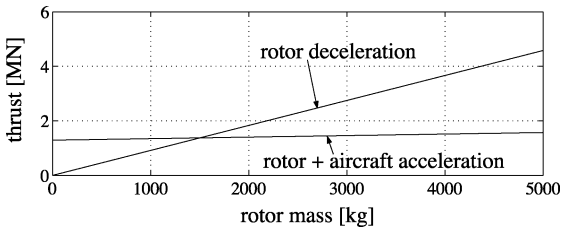

Fig. 1. Thrust required for acceleration and deceleration given as a function of rotor mass.

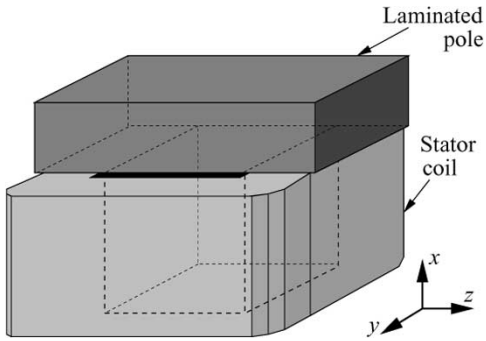

Fig. 2. One modular segment of the stator composed of a laminated pole/tooth enveloped by an armature coil.

mass. If the necessary calculations are carried out, the required value of acceleration and time length of the acceleration period are found to be 56.01 m/s^2 and 1.84 s, respectively. Similarly, required deceleration and the length of the deceleration periods to bring the rotor from its highest speed of 103 m/s to a stop within a distance of 5.79 m are found to be 916.2 m/s^2 and 0.112 s, respectively. The required force or thrust F that must be provided by the EMALS for acceleration and deceleration is given in Fig. 1 as a function of the rotor mass.

In Fig. 1, results presented show that a thrust of 2 MN is sufficient to accelerate aircraft and rotor, if rotor mass is less than 5000 kg. With the same thrust only rotors with a mass less than 2183 kg can be stopped within the prescribed distance. Thus, not considering the required power electronics supply and its limitations, a motor should be designed which is able to produce a thrust of 2 MN with a rotor mass less than 2183 kg.

III. Design of Linear Permanent Magnet Synchronous Motor and Linear Induction Motor

The basic design principle is to fabricate both the linear permanent magnet synchronous motor (LPMSM) and the linear induction motor (LIM) from modular stator segments. The concept is shown in idealized fashion in Fig. 2. Coordinate z is assumed to be the direction of motion, coordinate y the vertical depth, and coordinate x the thickness of the motor (direction of the air gap).

In general, each stator segment is composed of a laminated pole (or stator tooth) and a concentrated armature winding enveloping the pole with emphasis on easy assembly and replacement. In normal terminology, each of these poles constitutes one stator "tooth" of an armature. In the case of a winding fault the stator segment associated with the fault can be quickly and

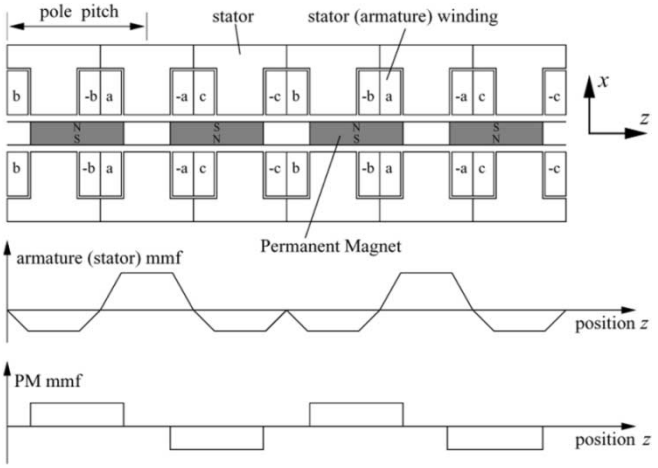

Fig. 3. HPP structure of LPMSM with the stator and rotor mmf waveforms ($i_a = I$, $i_b = -0.5I$, and $i_c = -0.5I$).

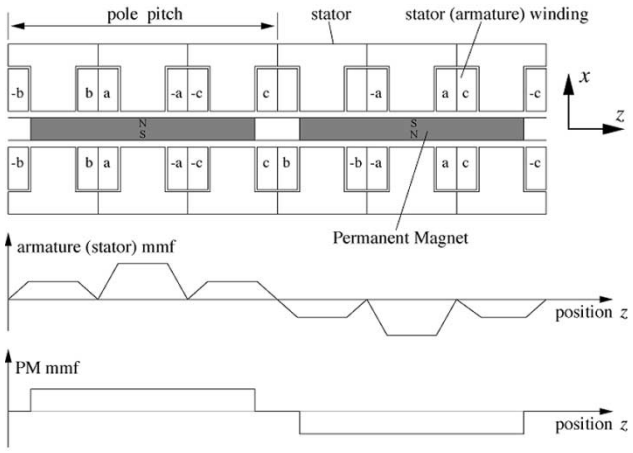

Fig. 4. OPP structure of LPMSM with the stator and rotor mmf waveforms ($i_a = I$, $i_b = -0.5I$, and $i_c = -0.5I$).

easily replaced with a new segment without disturbing the adjacent healthy segments. Two poles of the complete stator are assembled as a string of these stator segments. The stator coils can be connected in a variety of ways to realize a three-phase magnetomotive force (mmf) with currents i_a, i_b, and i_c in the three phases. From many possible connections of the stator coils only two are sufficiently promising to be discussed here. The first connection of the stator coils is the "1/2 phase per pole (HPP)" stator structure. This structure is shown in Fig. 3 for the LPMSM together with the corresponding armature and permanent magnet (PM) mmf waveforms. The second connection of the stator coils is the "one phase per pole (OPP)" stator structure. This arrangement is shown in Fig. 4 for the LPMSM together with the corresponding armature and PM mmf waveforms. In both cases presented here, the permanent magnets are embedded into the rotor frame that consists of nonmagnetic and nonconducting material. In the case of the LIM, the permanent magnet rotor is replaced by a massive copper sheet, while the stator HPP or OPP structures and their mmfs remain the same as in the case of LPMSM.

The proposed realization of the LPMSM for the EMALS is schematically presented in Fig. 5. Specifically, four independent stators (HPP or OPP) are oriented vertically and act on a single rotor with embedded permanent magnets. The system is

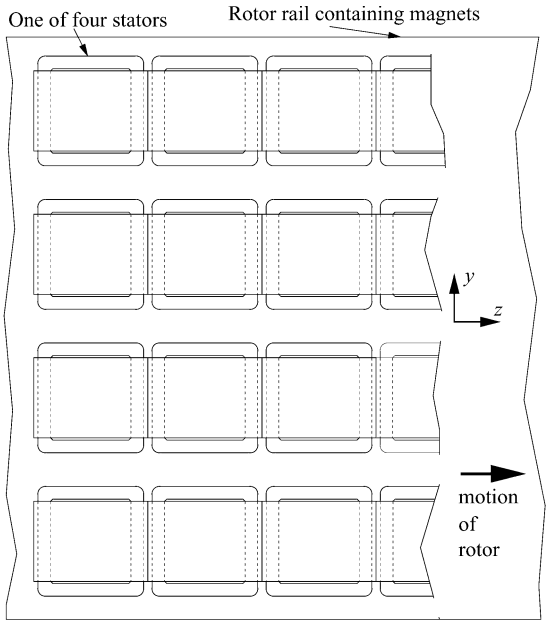

Fig. 5. Proposed four-stator-single-rotor realization of the LPMSM for the EMALS.

designed with sufficient redundancy such that in the case of removal of one of the four stators, the remaining three stators will be sufficient to produce 2 MN, which is enough for an aircraft launch. The realization of the LIM differs from the described LPMSM realization only in the rotor portion, which is made of a single copper sheet.

The design parameters of the HPP and OPP stator structures are given in Table I for the LPMSM and in Table II for the LIM.

TABLE I
PHYSICAL, OPERATIONAL, AND EQUIVALENT CIRCUIT PARAMETERS FOR THE LPMSM

PM Geometry	**HPP**	**OPP**
Thickness (mm)	37.8	25.4
Length in z direction (mm)	47.0	54.6
Length in y direction (mm)	500	500
Iron Core Geometry		
Pole pitch (mm)	72.4	73.8
Slot pitch (mm)	48.2	24.6
Tooth width (mm)	24.4	13.7
Slot opening (mm)	23.8	10.9
Tooth height (mm)	26.3	38.6
Yoke height (mm)	12.2	13.7
Air gap (mm)	6.5	6.5
Coil Geometry		
Coil width (mm)	11.9	5.4
Coil height (mm)	26.3	38.6
Coil length (mm)	500	500
Number of turns	1	1
Currents and Field Density		
Maximum current density (A/mm^2)	35	35
Phase current amplitude (kA)	10.744	7.271
Phase current RMS value (kA)	7.597	5.141
B_{max} in the air gap at load (T)	0.88	1.16
B_{max} in the tooth (T)	1.74	2.09
Rotor length and mass		
Total rotor length (m)	5.64	7.38
Total rotor height (m)	2.14	2.13
Total rotor mass (kg)	2093	2104
Operational and equivalent circuit parameters per coil		
Synchronous speed (m/s)	103	103
Frequency corresponding to final speed (Hz)	711.7	697.8
Primary coil ohmic resistance (μΩ)	120	160
Magnetizing inductance (μH)	0.229	0.469
Magnetizing reactance (mΩ)	1.024	2.052
Leakage inductance (μH)	0.695	0.746
Leakage reactance (mΩ)	3.107	3.271
Power factor Cos ϕ (at speed 103 m/s)	0.671	0.642

IV. DESIGN OF LINEAR BULK SUPERCONDUCTOR MAGNET MOTOR (LBSCMM)

The design of a LBSCMM is similar to the design of LPMSM. The permanent magnets used in the LPMSM are, in this case, replaced by sets of BSCs placed side by side. Each BSC is a field-cooled block of YBCO material with very high trapped magnetic field. Since the BSCs may produce flux densities above 2 T, an iron stator core cannot be used in the LBSCMMs due to saturation. In the absence of an iron core it is considered wise to use a conventional lap armature (stator) winding in order to develop a relatively undistorted sinusoidal position dependent thrust distribution. A cross section of the LBSCMM is shown in Fig. 7 given for two pole pitches. The rotor BSC magnets are alternately oriented in directions N-S and S-N and placed in an electrically and magnetically nonconductive material (e.g., fiberglass composite or Kevlar). The rotor is situated between two three-phase armature (stator) lap windings placed in the air.

The armature conductors with rectangular cross sections shown in Figs. 6–8 must be connected in the proper way to obtain the three-phase armature winding. Each armature coil has only one turn and consists of two conductors shown in Fig. 7 and the connection between them. The winding for each of the three phases consists of coils belonging to the same phase, which are connected in series or in parallel. The connection depends on the three-phase voltages and currents that can be provided by the electronic power converter. The three-phase windings are supplied by three symmetrical sinusoidal currents i_a, i_b, and i_c defined later in (6). Because the final decision about how to connect the phase coils has not been made yet, all results presented are given per phase or per two poles, while the connections between conductors and coils together with the real three-phase bus in Figs. 6–9 are denoted with the word bus.

Considering the maximal available size of the BSC magnets at the present state of art, eight BSC magnets ($x = 40$ mm, $y = 60$ mm, $z = 60$ mm) must be placed side by side in the y direction to reach the required motor height, as shown in Fig. 6. The machine cross section in the $y-z$ plane is shown in Fig. 8, where cuts of the bus and the armature conductors are marked by dashed lines.

A portion of the complete motor is shown in Fig. 9. It consists of four independent motors shown in Figs. 6–8. As in the previous LIM and LPMSM designs, four independent stators (armatures) act on a single rigid rotor that consists of four rotor substructures with BSCs presented in Figs. 6–8. Use of only three of the four motors must be sufficient to produce the required thrust of 2 MN. Each of four motors is closed loop controlled and supplied by an independent converter. In the case of fault the motor associated with the fault is switched off. Its terminals open and disable production of any braking or asymmetric forces. The remaining three motors are able to produce continuous and smooth thrust trajectory required to finish the launch process. The forces in the axes x and y are very small and can be neglected.

TABLE II
PHYSICAL, OPERATIONAL, AND EQUIVALENT CIRCUIT PARAMETERS FOR THE LIM

Secondary Geometry	**HPP**	**OPP**
Thickness of the Cu sheet (mm)	20	10
Length in z direction (mm)	530	1300
Length in y direction (mm)	710	710
Iron Core Geometry		
Pole pitch (mm)	265	650
Slot pitch (mm)	177	217
Tooth width (mm)	76	94
Slot opening (mm)	100	123
Tooth height (mm)	57	215
Yoke height (mm)	38	94
Length in y direction (mm)	500	500
Air gap (mm)	6.5	6.5
Coil Geometry		
Coil width (mm)	50	62
Coil height (mm)	57	215
Coil length (mm)	500	500
Number of turns	1	1
Maximum current density (A/mm^2)	35	35
Phase current amplitude (kA)	99.52	459.06
Phase current RMS value (kA)	70.37	324.60
Rotor length and mass		
Total rotor length (m)	4.24	7.80
Total rotor height (m)	3.31	3.96
Total rotor mass (kg)	2175	2070
Operational and equivalent circuit parameters per coil		
Rated slip	0.037	0.027
Synchronous speed (m/s)	108	108
Frequency corresponding to final speed (Hz)	204	83
Primary coil ohmic resistance (μΩ)	37.2	8.87
Magnetizing inductance (μH)	2.694	0.426
Magnetizing reactance (mΩ)	3.45	0.22
Leakage inductance (μH)	0.383	0.414
Leakage reactance (mΩ)	0.981	0.433
Power factor Cos ϕ (at speed 103 m/s)	0.504	0.106

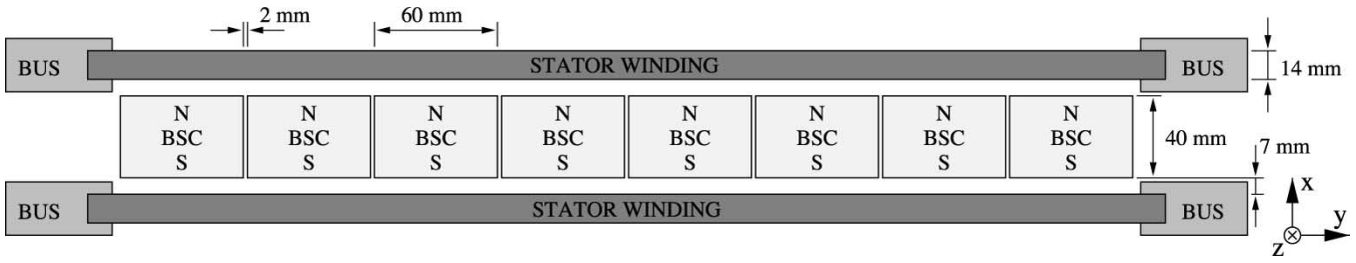

Fig. 6. Cross section of the LBSCMM in $x - y$ plane.

A. Modeling of the BSC Magnet and Calculation of Flux Density Distribution

The flux density distribution produced by a BSC is determined numerically by the "sand-pile model" in combination with the Biot–Savart law [19]. The sand-pile model of the BSC is schematically shown in Fig. 10. It is assumed that the currents flow along the edges so that square current loops are formed. The complete area of the BSC is divided into rectangular current loops that are placed in more layers. The cross section of each current loop is given by the height h and width w.

The current in one current loop is given by (2), where J_c is the critical current density in the BSC

$$I = J_c h w. \tag{2}$$

The complete volume of the BSC is divided into N_L layers with N_C current loops in each layer. Each current loop is approximated with an infinitely thin conductor in the middle of the current loop carrying current I. The differential of flux density vector $d\mathbf{B}$ generated by the current I carrying element of conductor $d\mathbf{s}$ is given by the Biot–Savart law

$$d\mathbf{B} = \frac{\mu_0 I}{4\pi} \frac{1}{||\mathbf{r}||^3} d\mathbf{s} \times \mathbf{r} \tag{3}$$

where μ_0 is the permeability of free space, $\mathbf{r}$ is the position vector of the current element vector $d\mathbf{s}$ to the point of observation, $\times$ denotes vector or cross product, while $||\mathbf{r}||$ denotes length of the vector $\mathbf{r}$. The flux density $\mathbf{B}$ at the point of observation is calculated by integration along all closed current loops in all layers.

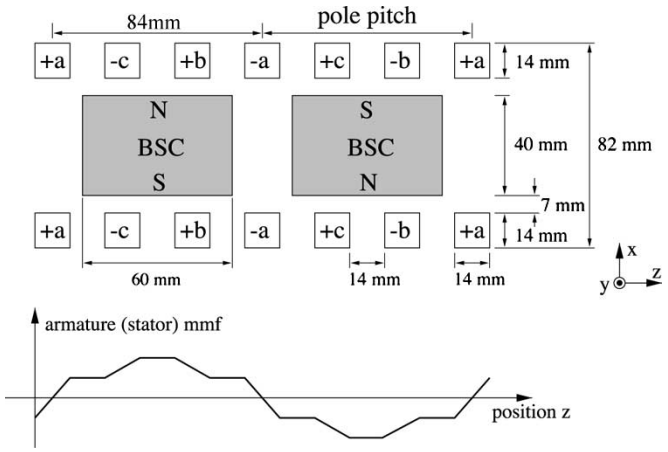

Fig. 7. Cross section of a LBSCMM in $x-z$ plane given for two pole pitches together with the stator mmf waveform ($i_a = I$, $i_b = -0.5I$, and $i_c = -0.5I$).

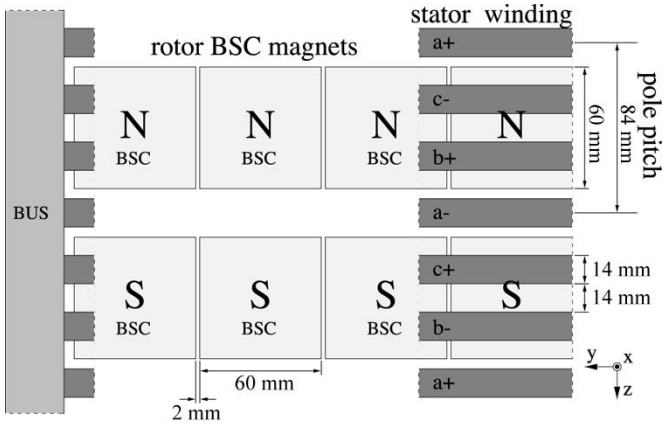

Fig. 8. Cross section of the LBSCMM in $y-z$ plane.

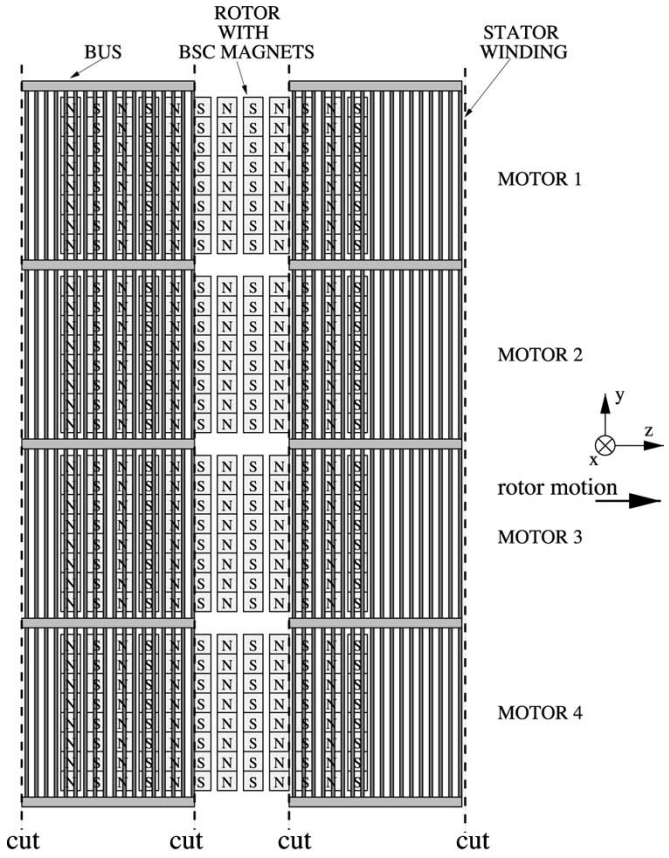

Fig. 9. Portion of the complete LBSCMM.

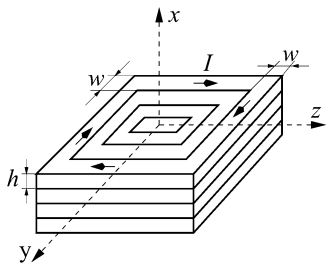

Fig. 10. Sand-pile model of a bulk superconductor (BSC).

In this work, the BSC is approximated by five current loops ($N_C = 5$) in four layers ($N_L = 4$). The approximation with infinitely thin conductors is shown in Fig. 11.

The BSC is located in the interval $-20 \leq x \leq 20$ mm, $-30 \leq y \leq 30$ mm, and $-30 \leq z \leq 30$ mm. The flux density vector component B_x in the plane placed 7 mm above the BSC surface ($x = 27$ mm) is shown in Fig. 12. It has been calculated by the BSC approximation shown in Fig. 11 for maximal current density in the BSC $J_C = 1000$ A/mm^2. This value is rather unusual for bulk YBCO superconductors at the present state. However, it is in the horizon and, as stated later in the paper, this current density assumption is made for lower temperatures.

The flux density vector component B_x produced by 16 BSCs arranged in two poles, as is shown in Figs. 7 and 8, is given in Fig. 13 for the plane placed 7 mm above the BSCs ($x = 27$ mm) for $J_C = 1000$ A/mm^2. The presented result has been calculated as the sum of appropriate displaced flux density distributions shown in Fig. 12 considering also the impact of BSCs located in the neighboring pole pairs.

To calculate the LBSCMM performances, the flux density vector $\mathbf{B} = [B_x, B_y, B_z]^T$ must be determined in the entire area where the armature winding is placed (in $-41 \leq x \leq -27$ mm and $27 \leq x \leq 41$ mm intervals). The flux density vector components B_x, B_y, and B_z are averaged with respect to the y axis in order to reduce the required computational effort. The averaged flux density vector components at different positions x above the BSCs are shown in Fig. 14. When properties of different BSCs differ due to the slightly different material properties, the flux density distribution shown in Fig. 13 can be slightly distorted, but the averaged flux densities shown in Fig. 14, and the overall LBSCMM performances cannot be substantially changed.

B. Force and emf Calculation

The force vector $d\mathbf{F}$, acting on an infinitely thin stator conductor element vector $d\mathbf{s}$ carrying stator current I_s, is given by

$$d\mathbf{F} = I_s d\mathbf{s} \times \mathbf{B}. \tag{4}$$

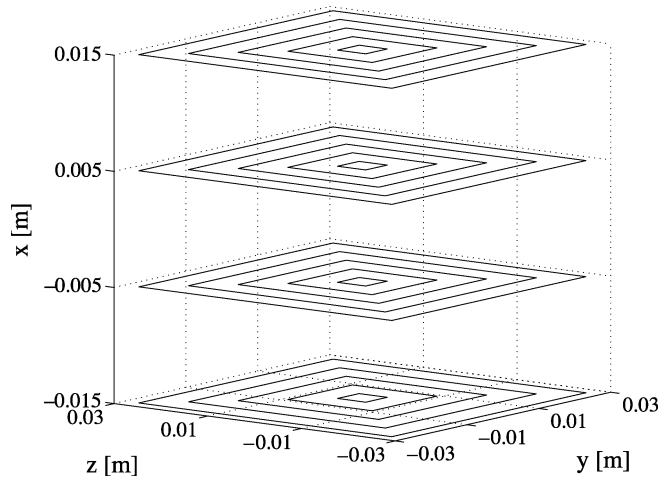

Fig. 11. BSC approximated with five infinitely thin conductors in four layers.

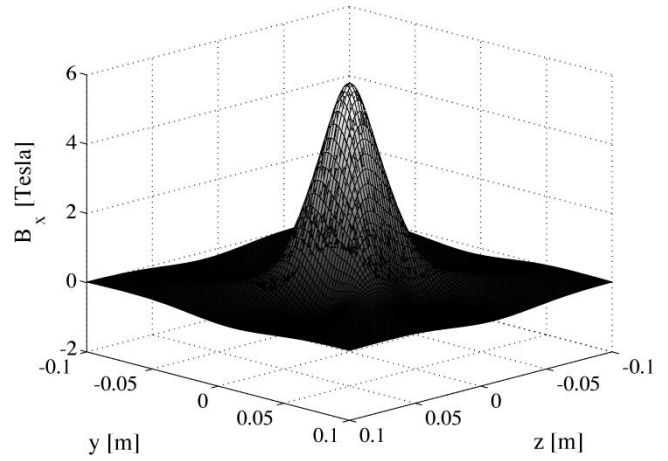

Fig. 12. Flux density B_x calculated 7 mm above the BSC surface at current density $J_C = 1000$ A/mm^2.

If the stator conductor cannot be considered as infinitely thin and the flux density vector $\mathbf{B}$ is averaged with respect to the axis y, then (4) leads to

$$d\mathbf{F} = J_s Y \mathbf{e}_s \times \mathbf{B}_{\text{av}}\, dA \tag{5}$$

where $\mathbf{B}_{\text{av}}$ is the flux density vector averaged with respect to the axis y, J_s is the current density in the stator conductor, Y is the conductor length in the y direction, $\mathbf{e}_s$ is the unity vector pointing in the direction of flowing current in the stator conductor, and dA is a differential element of the stator conductor cross section. The total force vector $\mathbf{F}$ produced by two poles of the LBSCMM can be calculated by integration over cross sections of all stator conductors shown in Fig. 7.

The force vector components F_z and F_x are shown in Fig. 15, together with the armature current sheet and flux density B_x. They are given for two poles of the stator shown in Fig. 7. The flux density B_x shown in Fig. 13 is produced by 16 BSC magnets arranged in two poles (eight in each pole), as shown in Figs. 6 and 8. The initial position of the rotor with BSC magnets is displaced by one pole pitch in the z direction with respect to the rotor position presented in Fig. 7. The phase a, phase b,

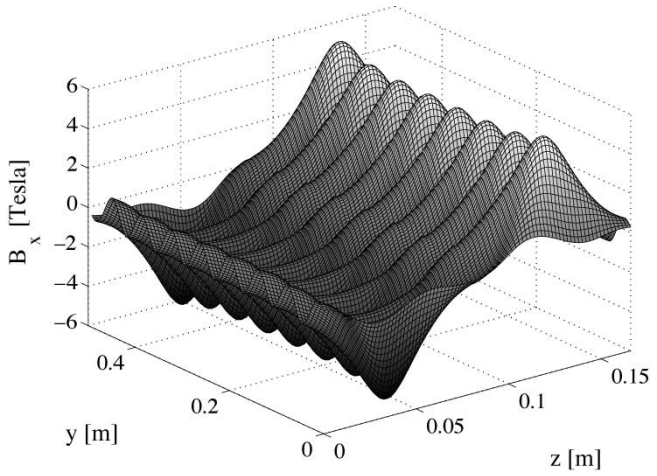

Fig. 13. Flux density B_x 7 mm above the BSC at $J_C = 1000$ A/mm^2 produced by 16 BSCs arranged in two poles considering impact of BSCs in six neighboring pole pairs.

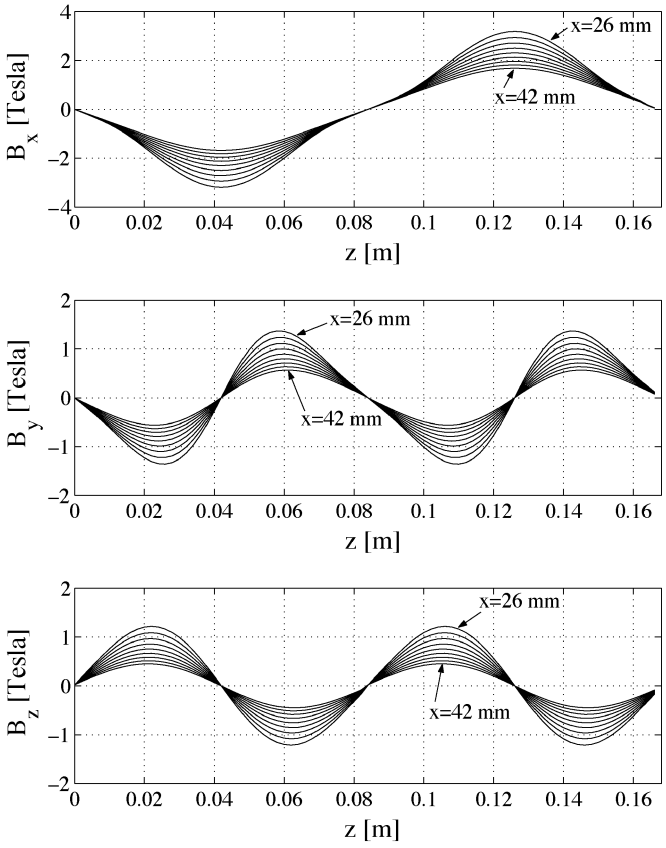

Fig. 14. Averaged flux densities B_x, B_y, and B_z given over two pole pitches for $x = 26, 28, 30, 32, 34, 36, 38, 40,$ and 42 mm and $J_C = 1000$ A/mm^2.

and phase c armature windings are, in general, supplied by sinusoidal currents i_a, i_b, and i_c

$$\begin{aligned} i_a &= I\cos(2\pi f t) \\ i_b &= I\cos\left(2\pi f t - \frac{2\pi}{3}\right) \\ i_c &= I\cos\left(2\pi f t - \frac{4\pi}{3}\right) \end{aligned} \tag{6}$$

where I is the amplitude of the sinusoidal currents, f is the frequency, while t denotes time. The results presented in Fig. 15 are given for the constant armature currents determined at the instant $t = 0$, while the rotor moves over two pole pitches. The distribution of armature conductors shown in Fig. 7, and the actual excitation with armature currents can be illustrated together by the armature current sheet shown in Fig. 15(a). It is given only for the upper set of armature conductors shown in Fig. 7.In the case of LBSCMM, the current sheet C_s can be determined for each armature conductor by (7)

$$C_s = \frac{i}{c_w\, c_h} c_h = J_s c_h = \frac{i}{c_w} \tag{7}$$

where i is the current in the conductor, while c_w and c_h are the conductor width and the conductor height, respectively. The armature mmf can be calculated by the integration of armature current sheet along the z axis. The averaged flux densities B_x, already shown in Fig. 14, are given in Fig. 15(b) for the initial rotor position, while they are given in Fig. 15(c) for the position where the peak value of the thrust F_z is reached. The force vector component F_x is shown in Fig. 15(d), while the thrust F_z is shown in Fig. 15(e).

The electromotive force (emf) induced in a single stator coil due to the magnetic field produced by the moving BSCs is calculated by

$$e_a = -\frac{d\psi_a}{dt} \tag{8}$$

where e_a is the phase a emf, ψ_a is the phase a flux linkage, while t denotes time. The emf induced in a single phase a coil is shown in Fig. 16 together with the corresponding flux linkage.

V. Results

Two different LBSCMM designs using the YBCO BSC magnets and considering the present state of the art in the field of YBCO HTS material have been carried out. In the first design the superconductor current density inside the magnet has been assumed to be 300 A/mm^2 at 77 K, corresponding to liquid nitrogen temperature. In the second design, the current density has been assumed to be 1000 A/mm^2. This is a very high current density that can be obtained only at low temperatures (below 40 K).

Table III shows the physical design parameters, equivalent circuit parameters, and operational parameters for both designs. Since the same stator structure is used in both designs, the equivalent circuit parameters are essentially equal. The only difference between the two designs is the rotor mass. Being able to operate at lower temperatures causes large air-gap fields and the required thrust can be obtained with much smaller rotor mass.

VI. Comparison of Different Motors for EMALS

Table IV summarizes the important data for all the three motors evaluated.

The motors presented have been evaluated with respect to the power factor $\cos(\phi)$, the rotor mass, and the armature time constant.

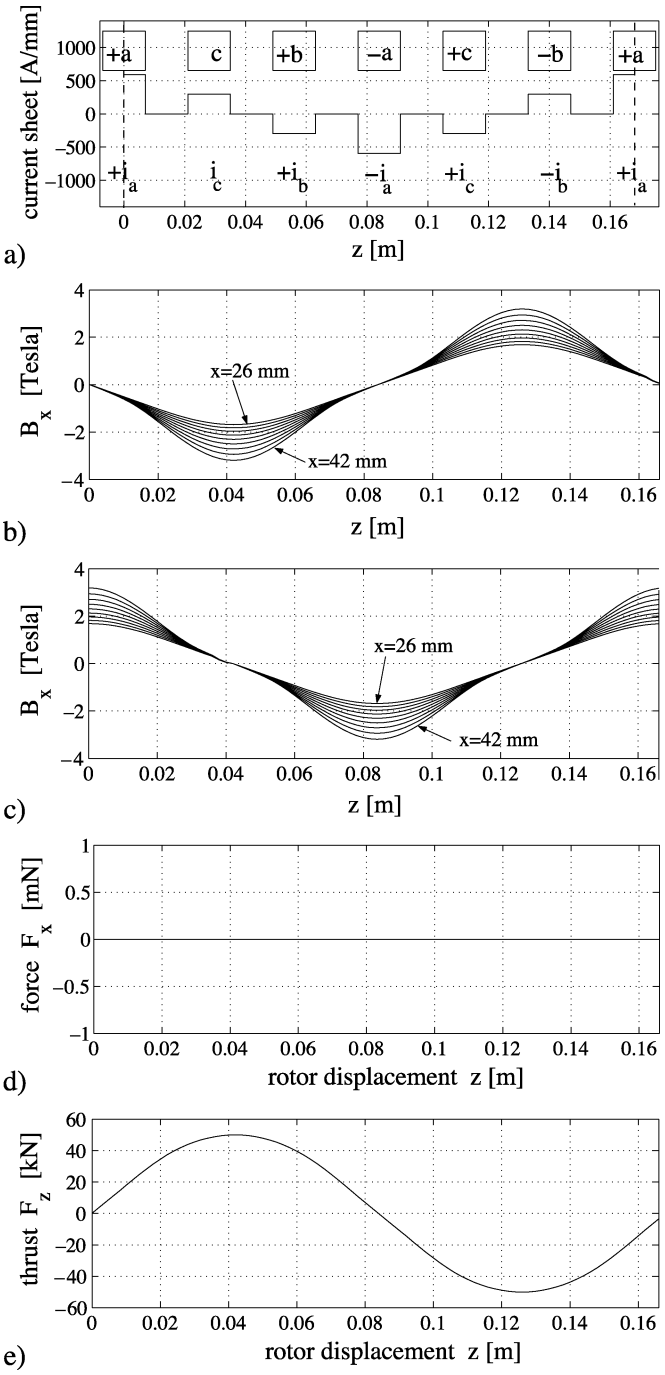

Fig. 15. (a) Armature conductors and armature current sheet produced by constant currents $i_a = 8316$ A, $i_b = i_c = -4158$ A. (b) Flux density B_x produced by 16 BSC magnets arranged in two poles at initial rotor position and BSC current density $J_C = 1000$ A/mm^2. (c) Flux density B_x produced by 16 BSC magnets arranged in two poles at peak value of the thrust F_z and BSC current density $J_C = 1000$ A/mm^2. (d) Force vector component F_x given for two poles when rotor moves over two-pole pitches. (e) Force vector component F_z acting on the stator given for two poles when rotor moves over two-pole pitches at constant armature currents.

The power factor is crucial for the design of power electronic conversion system and therefore one of the most important factors for evaluation of motors for EMALS. The development and operating costs of the power electronic conversion system can be substantially reduced if the power factor is almost unity. It must be noted that motors for EMALS do not operate in steady

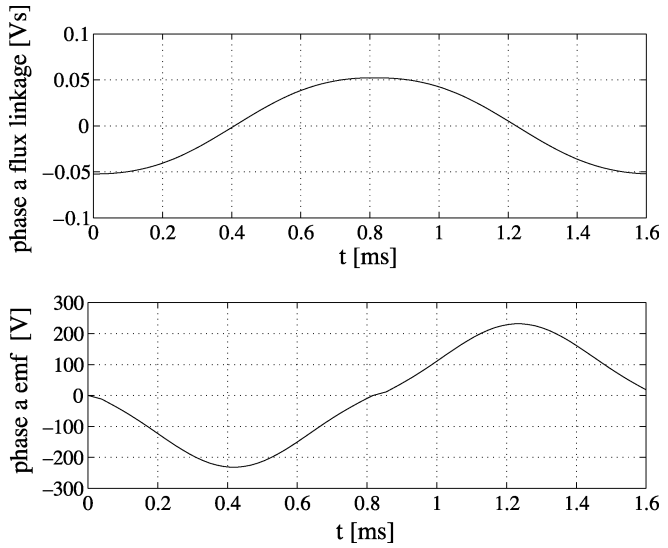

Fig. 16. Phase a flux linkage and emf caused by the rotor moving at speed $v = 103$ m/s (BSC current density $J_C = 1000$ A/mm^2).

TABLE III
PHYSICAL, OPERATIONAL, AND EQUIVALENT CIRCUIT PARAMETERS FOR THE LBSCMM

Temperature and critical current density	**77 K and 300 A/mm^2**	**40 K and 1000 A/mm^2**
BSC Geometry		
Thickness (cm)	4	4
Length in z direction (cm)	6	6
Length in y direction (cm)	6	6
Pole pitch (m)	0.084	0.084
Number of BSCs in one pole	8	8
Coil Geometry		
Coil cross-section width (m)	0.014	0.014
Coil cross-section height (m)	0.014	0.014
Coil length (m)	0.492	0.492
Number of turns	1	1
Maximum current density (A/mm^2)	30	30
Rotor length and mass		
Total rotor length (m)	6.38	2.35
Total rotor height (m)	2.14	2.14
Total rotor mass (kg)	2485	916
Operational and equivalent circuit parameters		
Synchronous speed (m/s)	103	103
Frequency corresponding to final speed (Hz)	613	613
Primary coil ohmic resistance (μΩ)	114	114
Inductance (μH)	0.052	0.052
Reactance (mΩ)	0.200	0.200
Power factor Cos ϕ (at speed 103 m/s)	0.999	0.999

state. Therefore, the power factor in Table IV is given for the maximal speed of 103 m/s and thrust of 2 MN.

According to the results shown in Fig. 1, only rotors with the mass less than 2183 kg can be stopped electromagnetically within the prescribed distance. Losses related with the energy transfer during acceleration and deceleration decrease with decreasing rotor mass. Because all motors presented produce thrust of 2 MN, the lower rotor mass means also better ratio thrust/(rotor mass) or Newtons per kilogram.

Losses in a coil depend on the resistance. The inductance and the resistance of the coil define the coil time constant. The complete coil behaves like a first-order element with the coil time constant. This time constant reduces the current ripple and limits the slope of the increasing current in the case of the fault. It is more difficult to design a power electronic conversion system with the prescribed current ripple if the coil time constant is too small.

TABLE IV
COMPARISON OF IMPORTANT DATA FOR LIM, LPMSM, AND LBSCMM DESIGNS TO OBTAIN A THRUST OF 2 MN

	LIM		**LPMSM**		**LBSCMM**	
	HPP	**OPP**	**HPP**	**OPP**	**77 K**	**Low T**
Pole pitch (m)	0.265	0.650	0.072	0.074	0.084	0.084
Rotor length in z (m)	4.24	7.8	5.64	7.38	6.38	2.35
Rotor height in y (m)	3.31	3.96	2.14	2.13	2.14	2.14
Total rotor mass (kg)	2175	2070	2093	2104	2485	916
Inductance of stator coil (μH)	3.077	0.840	0.924	1.215	0.052	0.052
Ohmic resistance of stator coil (μΩ)	37.2	8.87	120	160	114	114
Frequency corresponding to 103 m/s	204	83	712	698	613	613
Cos ϕ (at speed 103 m/s)	0.504	0.106	0.671	0.642	0.999	0.999

It can be seen from Table IV that LPMSM has a clear advantage over the LIM for this application. Although LPMSM has higher copper losses, its power factor is far superior translating to a substantial reduction in the cost of the associated power electronic conversion system. When BSC magnets are employed in the linear motor, an almost unity power factor can be obtained which would result in a dramatic reduction in the size and cost of the power electronic converters. However, at liquid nitrogen temperature (77 K), the LBSCMM does not seem to be a candidate at this point, even though it is superior to the other two motors. The reason for this is its somewhat limited peak flux density of the magnets (2 T) and the relatively heavy rotor. On the other hand, if the temperature can be reduced even further to around 40 K (or the BSC flux density increased by some other means), a much smaller rotor mass is obtained and such a LBSCMM could become a viable alternative in the future. However, the extremely low inductance presented by this type of motor to the power converter is a cause for concern. The LBSCMM has another advantage over the presented LPMSM and LIM designs in that the thrust distribution is almost sinusoidal. Of course, the permanent magnets used in the LPMSMs and the BSCs used in LBSCMMs may not substantially change their mechanical and magnetic properties due to deceleration with 916.2 m/s^2.

VII. CONCLUSION

Three different linear motor designs for EMALS have been evaluated and the results have been discussed. It has been concluded that at the present state of the art of the technology, the LPMSM is the best alternative, although better results have been obtained for an advanced LBSCMM. It is very likely that technological developments will yield newer materials that can trap higher magnetic fields, while the cost of cryogenic operations will continue to be reduced. In this case, the LBSCMM combined with a suitable power electronic converter may be the best candidate for this application in the long term.

REFERENCES

[1] M. K. Wu, J. R. Ashburn, C. J. Torng, P. H. Hor, R. L. Meng, L. Gao, Z. J. Huang, and C. W. Chu, "Superconductivity at 93 K in a new mixed-phase Y-Ba-Cu-O compound system at ambient pressure," *Phys. Rev. Lett.*, vol. 58, no. 9, pp. 908–910, 1987.

[2] W. V. Hassenzahl, "Superconductivity, an enabling technology for 21st century power systems?," *IEEE Trans. Appl. Superconduct.*, vol. 11, pp. 1447–1453, Mar. 2001.
[3] J. R. Hull, "Superconducting bearings," *Superconduct. Sci. Technol.*, vol. 13, pp. R1–R15, 2000.
[4] M. Murakami, "Measurement of trapped-flux density for bulk high-temperature superconductors," *Phys. C*, vol. 357–360, pp. 751–754, 2001.
[5] H. M. Wen, L. Z. Lin, L. Y. Xiao, L. Xiao, Y. L. Jiao, M. H. Zheng, and H. T. Ren, "Trapped field magnets of high-Tc superconductors," *IEEE Trans. Appl. Superconduct.*, vol. 10, pp. 898–900, Mar. 2000.
[6] S. Gruss, G. Fuchs, G. Krabbes, P. Verges, P. Schatzle, K. H. Muller, J. Fink, and L. Schultz, "Trapped fields beyond 14 Tesla in bulk YBa2Cu3O7-d," *IEEE Trans. Appl. Superconduct.*, vol. 11, pp. 3720–3723, Mar. 2001.
[7] H. Ikuta, A. Mase, Y. Yanagi, M. Yoshikawa, Y. Itoh, T. Oka, and U. Mizutani, "Melt-processed Sm-Ba-Cu-O superconductors trapping strong magnetic field," *Superconduct. Sci. Technol.*, vol. 11, pp. 1345–1347, 1998.
[8] T. Miyamoto, K. Nagashima, N. Sakai, and M. Murakami, "Mechanical properties of bulk superconductors," *Superconduct. Sci. Technol.*, vol. 13, pp. 816–819, 2000.
[9] Y. Sanagawa, H. Ueda, M. Tsuda, A. Ishiyama, S. Kohayashi, and S. Haseyama, "Characteristics of lift and restoring force in HTS bulk—Application to two-dimensional maglev transporter," *IEEE Trans. Appl. Superconduct.*, vol. 11, pp. 1797–1800, Mar. 2001.
[10] R. Muramatsu, S. Sadakata, M. Tsuda, and A. Ishiyama, "Trial production and experiments of linear actuator with HTS bulk secondary," *IEEE Trans. Appl. Superconduct.*, vol. 11, pp. 1976–1979, Mar. 2001.
[11] L. K. Kovalev, K. V. Ilyushin, V. T. Penkin, K. L. Kovalev, S. M. A. Koneev, K. A. Modestov, S. A. Larionoff, W. Gawalek, and B. Oswald, "Electrical machines with bulk HTS elements—The achieved results and future development," *Phys. C*, vol. 357–360, pp. 860–865, 2001.
[12] G. J. Barnes, M. D. McCulloch, and D. Dew-Hughes, "Applications and modeling of bulk HTS's in brushless ac machines," *Superconduct. Sci. Technol.*, vol. 13, pp. 875–878, 2000.
[13] A. L. Rodrigues, "New electric reluctance motor with bulk superconducting materials on the rotor," in *Conf. Rec. Third Int. Aegean Conf. Electric Machines and Power Electronics (ACEMP)*, Kusadasi, Turkey, 2001, pp. 656–660.
[14] C. E. Oberly, G. Kozlowski, C. E. Gooden, R. X. Lenard, A. K. Sarkar, I. Maartense, and J. C. Ho, "Principles of application of high temperature superconductors to electromagnetic launch technology," *IEEE Trans. Magn.*, vol. 27, pp. 509–514, Mar. 1991.
[15] M. R. Doyle, D. J. Samuel, T. Conway, and R. R. Klimowski, "Electromagnetic aircraft launch system—EMALs," *IEEE Trans. Magn.*, vol. 31, pp. 528–533, Mar. 1995.
[16] H. D. Fair, "The science and technology of electric launch," *IEEE Trans. Magn.*, vol. 37, pp. 25–32, Mar. 2001.
[17] R. R. Bushway, "Electromagnetic aircraft launch system development considerations," *IEEE Trans. Magn.*, vol. 37, pp. 52–54, Mar. 2001.
[18] R. J. Elwell, R. W. Garman, and M. Doyle, "Thermal management techniques for an advanced linear motor in an electric aircraft recovery system," *IEEE Trans. Magn.*, vol. 37, pp. 476–479, Mar. 2001.
[19] H. Fukai, M. Tomita, M. Murakami, and T. Nagatomo, "Numerical simulation of trapped magnetic field for bulk superconductor," *Phys. C*, vol. 357–360, pp. 774–776, 2001.

Gorazd Štumberger (M'92) was born in 1964 in Ptuj, Slovenia. He received the B.S., M.Sc., and Ph.D. degrees in electrical engineering from the University of Maribor, Maribor, Slovenia, in 1989, 1992, and 1996, respectively.

In 1989, he joined the Faculty of Electrical Engineering and Computer Science, University of Maribor, where he currently is an Associate Professor. He was as a Visitor with the University of Wisconsin, Madison, in 1997 and 2001, and with the Kaholieke Universiteit Leuven, Belgium, in 1998 and 1999. His current research interests include design, modeling, analysis, and control of electrical machines.

Mehmet Timur Aydemir (SM'92–M'95) was born in 1962 in Turkey. He received the B.Sc. degree in 1983 and M.Sc. degree in 1985, from Karadeniz Technical University, both in electrical and electronics engineering. He received the Ph.D. degree from the University of Wisconsin, Madison, in 1995.

He worked as a Research Assistant at Karadeniz Technical University. He has been working at Gazi University, Ankara, Turkey, as an Assistant Professor since 1995. From 2001 to 2002, he was a Visiting Researcher at the University of Wisconsin, Madison, on a Fulbright Scholarship. His research interests include power electronics and electrical machines.

Dr. Aydemir won a scholarship from the Ministry of Education of Turkey for Ph.D. education in the USA in 1988.

Damir Žarko was born in Zagreb, Croatia, on September 28, 1972. He received the B.S. and M.S. degrees in electrical engineering from the University of Zagreb in 1995 and 1999, respectively. He is currently working toward the Ph.D. degree at the University of Wisconsin, Madison,

From 1995 to 2000, he was an Assistant at the Department of Electrical Machines Drives and Automation, Faculty of Electrical Engineering and Computing, University of Zagreb, where his research interests included numerical analysis of large synchronous generators and power transformers. Since June 2000, he has been a Research Assistant at the University of Wisconsin, Madison.

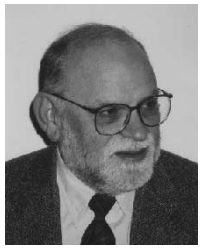

Thomas A. Lipo (M'64–SM'71–F'87) was born in Milwaukee, WI. He received the B.E.E. and M.S.E.E. degrees from Marquette University, Milwaukee, in 1962 and 1964, respectively, and the Ph.D. degree in electrical engineering from the University of Wisconsin, Madison, in 1968.

From 1969 to 1979, he was an Electrical Engineer in the Power Electronics Laboratory of Cooperate Research and Development, General Electric Company, Schenectady, NY. He became a Professor of Electrical Engineering at Purdue University, West Lafayette, IN, in 1979, and in 1981, he joined the University of Wisconsin, Madison, in the same capacity, where he is presently the W. W. Grainger Professor for Power Electronics and Electrical Machines.

Dr. Lipo has received the Outstanding Achievement Award from the IEEE Industry Applications Society (IAS), the William E. Newell Award of the IEEE Power Electronics Society, and the 1995 Nicola Tesla IEEE Field Award from the IEEE Power Engineering Society for his work. He has served IEEE in various capacities, including President of the IAS. He is a Fellow of the Institution of Electrical Engineers, U.K., and the Royal Academy of Great Britain as well as a Member of the Institute of Electrical Engineers of Japan.